Signal Processing 30 (1993) 141–162
Elsevier

A family of polynomial spline wavelet transforms

Michael Unser, Akram Aldroubi and Murray Eden

Biomedical Engineering and Instrumentation Program, National Center for Research Resources, National Institutes of Health, Bethesda, MD 20892, USA

Received 25 July 1991
Revised 24 January 1992 and 25 May 1992

Abstract. This paper presents an extension of the family of orthogonal Battle/Lemarié spline wavelet transforms with emphasis on filter bank implementation. Spline wavelets that are not necessarily orthogonal within the same resoluton level, are constructed by linear combination of polynomial spline wavelets of compact support, the natural counterpart of classical *B*-spline functions. Mallat's fast wavelet transform algorithm is extended to deal with these non-orthogonal basis functions. The impulse and frequency responses of the corresponding analysis and synthesis filters are derived explicitly for polynomial splines of any order n (n odd). The link with the general framework of biorthogonal wavelet transforms is also made explicit. The special cases of orthogonal, *B*-spline, cardinal and dual wavelets are considered in greater detail. The *B*-spline (respectively dual) representation is associated with simple FIR binomial synthesis (respectively analysis) filters and recursive analysis (respectively synthesis) filters. The cardinal representation provides a sampled representation of the underlying continuous functions (interpolation property). The distinction between cardinal and orthogonal representation vanishes as the order of the spline is increased; both wavelets tend asymptotically to the bandlimited sinc-wavelet. The distinctive features of these various representations are discussed and illustrated with a texture analysis example.

Zusammenfassung. Dieser Artikel stellt eine Verallgemeinerung der Familie der orthogonalen Spline-Wavelet-Transformationen nach Battle/Lemarié vor, wobei insbesondere auf die Filterbank-Implementierung eingegangen wird. Durch Linearkombination von Polynom-Spline-Wavelets mit kompaktem Träger – dem natürlichen Gegenstück zu klassischen *B*-Spline-Funktionen – werden Spline-Wavelets konstruiert, die nicht notwendigerweise orthogonal innerhalb eines Auflösungsniveaus sind. Der schnelle Wavelet-Transformations-Algorithmus von Mallat wird auf diese nichtorthogonalen Basisfunktionen erweitert. Die Impulsant worten und Übertragungsfunktionen der zugeordneten Analyse- und Synthesefilter werden für Polynom-Splines beliebiger (ungerader) Ordnung explizit hergeleitet. Die Verbindung zum allgemeinen Konzept der biorthogonalen Wavelet-Transformationen wird ebenfalls klar herausgearbeitet. Die Spezialfälle der orthogonalen, *B*-Spline-, kardinalen und dualen Wavelets werden im Detail betrachtet. Die *B*-Spline- (bzw. duale) Darstellung ist mit einfachen nichtrekursiven binomialen Synthesefiltern (bzw. Analysefiltern) sowie rekursiven Analysefiltern (bzw. Synthesefiltern) verbunden. Die kardinale Darstellung ergibt eine abgetastete Darstellung der zugrundeliegenden kontinuierlichen Funktion (interpolationseigenschaft). Bei zunehmender Ordnung des Splines verschwindet der Unterschied zwischen der kardinalen und der orthogonalen Darstellung; beide Wavelets nähern sich dem bandbegrenzten sinc-Wavelet an. Die charakteristischen Merkmale dieser verschiedenen Darstellungen werden diskutiert und durch ein Texturanalyse-Beispiel illustriert.

Résumé. Ce papier présente une extension de la famille orthogonale d'ondelettes spline de Battle et Lemarié en mettant l'accent sur une mise en oeuvre par banc de filtres. Des ondelettes spline – pas forcément orthogonales à l'intérieur d'un même niveau de resolution – sont construites par convolution discrète d'ondelettes spline polynomiales à support compact; ces dernières étant l'extension naturelle des fonctions *B*-spline classiques. L'algorithme de décomposition et reconstruction par filtrage QMF de Mallat est modifié pour ces fonctions de bases non-orthogonales. Les réponses impulsionelles et fréquentielles des filtres

Correspondence to: Dr. Michael Unser, BEIP/NCRR, Building 13, Room 3W13, National Institutes of Health, Bethesda, Maryland 20892, USA. Tel: (301) 496-4426; Fax: (301) 496-6608; E-Mail: unser@helix.nih.gov.

Elsevier Science Publishers B.V.

correspondant d'analyse et de synthèse sont déterminées de façon explicite pour tout les splines polynomiaux d'ordre impaire. Le lien avec la théorie générale des ondelettes biorthogonales est aussi établi. Les cas particuliers des ondelettes spline orthogonales, B-spline, cardinales et duales sont traités de façon plus approfondie. La représentation B-spline (resp. duale) donne lieu à de simples filtres binomiaux de synthèse (resp. d'analyse) et des filtres récursifs d'analyse (resp. synthèse). La représentation cardinale correspond à une représentation échantillonnée des fonctions continues sous-jacentes (propriété d'interpolation). La distinction entre représentation cardinale et orthogonale s'atténue lorsque le degré des fonctions spline augmente; ces deux types d'ondelettes convergent vers une même fonction sinc modulée lorsque l'ordre tend vers l'infini. Les propriétés de ces diverses représentations sont mises en évidence en s'appuyant sur un exemple d'analyse de texture.

Keywords. Wavelet transform; B-splines; polynomial splines; interpolation; binomial filters; quadrature mirror filters (QMF); biorthogonality; multiresolution signal analysis.

1. Introduction

The wavelet decomposition of a continuous-time signal $g(x)$ is an expansion of the form

$$g(x)=\sum_{i\in\mathbb{Z}}\sum_{k\in\mathbb{Z}} d_{(i)}(k)\psi(2^{-i}x-k), \tag{1.1}$$

where the basis functions are generated by dilation (index i) and translation (index k) of a single prototype $\psi(x)$. The wavelet function $\psi(x)$ must satisfy certain properties such that there exists a linear one-to-one mapping between a function $g(x)\in L_2$ and its wavelet coefficients $\{d_{(i)}(k), (i,k)\in\mathbb{Z}^2\}$; this mapping defines the discrete wavelet transform [10, 25, 29]. This type of representation has a number of attractive features that have contributed to its recent growth in popularity among mathematicians and signal processors [33, 40]. First, it is a hierarchical decomposition that enables the characterization of signal over scale (multiresolution analysis) [24, 25]. Second, the wavelet transform is in essence a subband signal decomposition; in fact, it is closely related to a variety of multirate decomposition techniques described in the signal processing literature [9, 39, 48, 52]. Finally, there is a fast reversible wavelet transform algorithm that uses quadrature mirror filter (QMF) banks [25].

Here we will consider the special case in which the basis functions are polynomial splines. Several such examples have played a significant role in the early development of the wavelet transform theory. The oldest one is the well known Haar transform [18], which corresponds to a spline of order $n=0$. The next example was constructed by Strömberg using one-sided polynomial splines of order n [41]. Later, Battle and Lemarié independently constructed orthogonal spline wavelets using symmetrical basis functions with an exponential decay [3, 21]. Another well known example is the modulated sinc-wavelet (ideal bandpass filter), which can be viewed as a spline of infinite order [21]. More recently, Chui and Wang introduced the B-spline wavelets of compact support [7], which are the natural counterparts of the classical B-splines [34, 35]. We did the same construction independently and also proved that the B-spline wavelets converge to a modulated Gaussian as the order of the spline goes to infinity [46].

The purpose of this paper is to unify these various approaches by developing a general framework for polynomial spline wavelet transform. We will introduce some general design principles and present some new examples of wavelet transforms; for example, the cardinal spline wavelet transform which has the fundamental interpolation property. We will also emphasize a signal processing point of view which should make these techniques more accessible to an engineering audience.

The presentation is organized as follows. In Section 2, we review some results on polynomial splines and discuss the concept of a spline pyramid. The wavelet transform essentially provides a non-redundant representation of the differences between adjacent levels in such a pyramid. In

Section 3, we show how to obtain such a representation by deriving the B-spline wavelets of compact support. We then use discrete convolution operators to specify an extended family of polynomial spline wavelet transforms. In particular, we demonstrate that the use of non-orthognal wavelets can simplify the filters and computations in the wavelet decomposition algorithm. Some of these filters are FIR binomial kernels and can be implemented using addition only, while others have a simple recursive structure. We also indicate how this family of spline transforms falls into the general framework of biorthogonal wavelet transforms [8, 19, 32, 50]. In this respect, we note that a distinctive feature of the present approach is the orthogonality of the wavelets across scales, a property that is usually not present in other biorthogonal schemes. Finally, in Section 5, we consider some image processing examples and discuss the properties of various representations.

Notation and operators

L_2 is the vector space of measurable, square-integrable one-dimensional functions $f(x)$, $x\in\mathbb{R}$. The inner product of $f(x)\in L_2$ with $g(x)\in L_2$ is denoted by $\langle f(x), g(x)\rangle$. l_2 is the space of square summable sequences (or discrete signals) $a(k)$, $k\in\mathbb{Z}$. We will consider a number of operators acting on discrete signals. A summary of these operations together with their effect in the z-transform domain is given in Table 1.

Table 1
Properties of the z-transform

Operator	Signal	z-transform
Discrete signal	$a(k)$	$A(z)=\sum_{k=-\infty}^{+\infty} a(k)z^{-k}$
Time shift	$a(k-k_0)=\delta_{k_0} * a(k)$	$z^{-k_0}A(z)$
Time reversal	$a'(k):=a(-k)$	$A(1/z)$
Modulation	$a(k):=(-1)^k a(k)$	$A(-z)$
Down-sampling	$[a]_{\downarrow m}(k)$	$\sum_{k=0}^{m-1} \frac{A([z\,e^{j2\pi k}]^{1/m})}{m}$
Up-sampling	$[a]_{\uparrow m}(k)$	$A(z^m)$
Convolution	$a * b(k)$	$A(z)B(z)$
Inverse filter	$(b)^{-1}(k)$	$B(z)^{-1}$
Square-root inverse	$(b)^{-1/2}(k)$	$B(z)^{-1/2}$

Superscript and subscript convention: The functions considered here are polynomial splines and typically bear two indices (e.g., $g^n_{(i)}(x)$, $\psi^n_{\mathrm{b}}(x)$). The superscript 'n' denotes the spline order and also the degree of the piecewise polynomial segments. The subscript in parentheses indicates a resolution level: (i) corresponds to a step size of 2^i. A subscript letter is used to indicate a particular type of scaling function or wavelet (e.g., o: orthogonal, b: B-spline, c: cardinal and d: dual).

2. Multi-resolution polynomial spline representations

We consider a sequence of nested polynomial spline function spaces $\{V^n_{(i)},\ i\in\mathbb{Z}\}$ of order n (n odd) such that $V^n_{(i)}\supset V^n_{(i+1)}$ for $i\in\mathbb{Z}$. Specifically, $V^n_{(i)}$ is the sub-set of functions in L_2 that are of class C^{n-1} (i.e. continuous functions with continuous derivatives up to order $n-1$) and are polynomials of degree n (n odd) on each interval $[k2^i, (k+1)2^i)$ with $k\in\mathbb{Z}$. These subspaces can be defined, as in [47], by

$$V^n_{(i)}=\left\{g^n_{(i)}(x)=\sum_{k=-\infty}^{+\infty} c_{(i)}(k)\varphi^n(2^{-i}x-k),\ x\in\mathbb{R},\ c_{(i)}\in l_2\right\}, \tag{2.1}$$

where the scaling function $\varphi^n(x)$ is a weighted sum of B-splines,

$$\varphi^n(x)=\sum_{k=-\infty}^{+\infty} p(k)\beta^n(x-k), \tag{2.2}$$

and where p is an arbitrary invertible convolution operator (or filter) from l_2 into itself. The function $\beta^n(x)$ is Schoenberg's central B-spline of order n; it can be constructed by repeated convolution of a B-spline of order 0:

$$\beta^n(x)=\underbrace{\beta^0 * \beta^0 * \cdots * \beta^0}_{n+1\text{ times}}(x), \tag{2.3}$$

where $\beta^0(x)$ is the characteristic function in the interval $[-\frac{1}{2}, \frac{1}{2})$. The subscript (i) that is used

throughout the presentation denotes the resolution level; it can be interpreted as a coarseness index. Increasing the resolution level corresponds to stretching the basis functions by a factor of two.

For $p=\delta_0$ (identity filter), the expansion in (2.1) is the standard B-spline representation [34, 35]. A fundamental characteristic of B-spline basis functions is their compact support, the property that makes them useful in a variety of applications [31].

The fact that the function spaces are nested implies that the basis functions at coarser levels are themselves included in the finer resolution spaces; i.e., $\beta^n(x)\in V^n_{(i)}$, $i\leqslant 0$. Specifically, we have the two scale relation

$$\beta^n(x/2)=\sum_{k=-\infty}^{+\infty} u_2^n(k)\beta^n(x-k), \tag{2.4}$$

where u_2^n is the binomial kernel of order n,

$$u_2^n(k)=\begin{cases}\dfrac{1}{2^n}\binom{n+1}{k+(n+1)/2}, & |k|\leqslant (n+1)/2,\\ 0, & \text{otherwise}\end{cases}$$

$$\xleftrightarrow{\text{DFT}} \quad U_2^n(f)=2\cos^{n+1}(\pi f). \tag{2.5}$$

This property fails for n even unless one uses modified spline functions spaces for which the basis functions are shifted by half a sampling step with respect to the origin. This difficulty does not arise if causal B-splines are used instead of centered basis functions, the approach taken by Chui and Wang [7]. We note, however, that the use of causal B-splines may create other complications because the corresponding cardinal spline interpolation problem for n even is ill-posed (cf. [43]).

Given a function $g(x)\in L_2$, we can obtain its minimum error polynomial spline approximation for all resolution levels $i\in\mathbb{Z}$. Such a sequence of fine-to-coarse approximations, $\{g^n_{(i)}(x)\}_{i\in\mathbb{Z}}$, defines a multiresolution analysis, called the polynomial spline pyramid. We have shown previously [47] that the coefficients of the polynomial spline pyramid can be constructed recursively by repeated application of a REDUCE function (filtering and down-sampling by a factor of 2):

$$c_{(i+1)}(k):=[\mathring{v} * c_{(i)}]_{\downarrow 2}(k), \tag{2.6}$$

where the impulse response of the prefilter $\mathring{v}$ is

$$\mathring{v}(k)=\tfrac{1}{2}[(p * b^{2n+1})^{-1}]_{\uparrow 2} * p * b^{2n+1} * u_2^n(k). \tag{2.7}$$

The sequence b^n denotes the discrete spline of order n, which is obtained by sampling the B-splines at the integers,

$$b^n(k)=\beta^n(x)|_{x=k} \quad \xleftrightarrow{z} \quad B_1^n(z). \tag{2.8}$$

Note that the filters b^n and u_2^n both have a finite impulse response (FIR).

Conversely, the coefficients of a signal approximation at a resolution level (i_0) can be expanded to any finer level $(i<i_0)$ by successive application of an EXPAND function (up-sampling and post-filtering). Specifically, the expansion coefficients $\hat{c}_{(i)}(k)$ of $g_{(i+1)}(x)$ in the standard representation (2.1) can be computed as

$$\hat{c}_{(i)}(k)=v * [c_{(i+1)}]_{\uparrow 2}(k), \tag{2.9}$$

where the postfilter is

$$v=[p]_{\uparrow 2} * u_2^n * (p)^{-1}. \tag{2.10}$$

The computational procedure described by (2.6) and (2.9) is an extension to non-orthogonal basis functions of Mallat's multiresolution approximation algorithm [25].

3. Polynomial spline wavelets

Let us denote by $r^n_{(i+1)}:=g^n_{(i)}-g^n_{(i+1)}$ the loss of information (or residue) resulting from the application of the REDUCE operation defined by (2.6). This residue can be represented in the difference pyramid, as suggested in [47], although such a representation has twice as many degrees of freedom as necessary. In two dimensions, this representation is overcomplete by a factor of 4/3. Here, we consider a more compact representation using the

wavelet transform concept proposed by Mallat, Meyer and others.

By construction, the residue $r^n_{(i+1)}$ is included in $V^n_{(i)}$, and is perpendicular to $V^n_{(i+1)}$; that is, $r^n_{(i+1)} \in W^n_{(i+1)}$, where $W^n_{(i+1)} \oplus V^n_{(i+1)} = V^n_{(i)}$ and $W^n_{(i+1)} \perp V^n_{(i+1)}$. $W^n_{(i+1)}$ is the so-called residual (or detail) space at resolution 2^{i+1}. The essence of the wavelet decomposition method is to construct sets of shift-invariant bases for the sequence of residual spaces: $\{W^n_{(i)}, i \in \mathbb{Z}\}$, so that

$$V^n_{(i)} = \bigoplus_{k=i+1}^{+\infty} W^n_{(k)} = V^n_{(I)} \oplus \left(\bigoplus_{k=i+1}^{I} W^n_{(k)} \right), \quad I > i \tag{3.1}$$

and

$$W^n_{(i)} \perp W^n_{(j)}, \quad (i,j) \in \mathbb{Z}^2 \text{ and } i \neq j. \tag{3.2}$$

Lemarié's solution uses orthogonal spline wavelets. He has shown that they have an exponential localization [21]. We show here that this construction method can be extended. For this purpose, we will initially set the framework of our representation to $p = \delta_0$ and construct polynomial spline wavelets with a compact support (ψ^n_b), which are the natural counterparts of the standard B-splines ($\varphi^n_b = \beta^n$) [34].

3.1. Spline wavelets of compact support

Specifically, we would like to find a wavelet of the form

$$\psi^n(x/2) = \sum_{k=-\infty}^{+\infty} w(k) \beta^n(x-k), \tag{3.3}$$

that is orthogonal to the set of expanded B-spline functions $\{\beta^n(x/2-k), k \in \mathbb{Z}\}$ with the additional constraint that the sequence $w(k)$ is finite. By using the representation of expanded basis function (2.4) together with the property $\langle \beta^n(x), \beta^n(x-y) \rangle = \beta^{2n+1}(y)$ (a direct consequence of (2.3)), the orthogonality constraint can be expressed as a convolution equation,

$$\langle \psi^n(x/2), \beta^n(x/2-k) \rangle = [w * u^n_2 * b^{2n+1}]_{\downarrow 2}(k) = 0 \quad \forall k \in \mathbb{Z}. \tag{3.4}$$

Taking the z-transform, we get

$$\frac{1}{2} \left(W(z) U^n_2(z) B^{2n+1}_1(z) + W(-z) U^n_2(-z) B^{2n+1}_1(-z) \right) = 0. \tag{3.5}$$

It can be verified by substitution that a general solution to this equation is

$$W(z) = z U^n_2(-z) B^{2n+1}_1(-z) Q(z^2),$$

where $Q(z)$ is an arbitrary polynomial in z. The sequence w of minimal length is obtained for $Q(z) = 1$. Taking the inverse z-transform (cf. rules in Table 1), we obtain an explicit formula for the B-spline wavelet of order n,

$$\psi^n_b(x/2) = \sum_{k=-\infty}^{+\infty} (\underline{u}^n_2 * \underline{b}^{2n+1} * \delta_{-1})(k) \beta^n(x-k), \tag{3.6}$$

where the notation $\underline{a}(k) := (-1)^k a(k)$ refers to a modulation by $(-1)^k$ and where $\delta_i(k)$ represents a unit pulse at position $k = i$ and acts as the shift operator: $\delta_i * a(k) = a(k-i)$. ψ^n_b is obtained from a weighted sum of basic B-splines and hence is a polynomial spline of order n (i.e. $\psi^n_b(x/2) \in V^n_{(0)}$). Based on the orthogonality property (3.4), we get the following theorem.

THEOREM 1. For $i \in \mathbb{Z}$, the vector spaces $W^n_{(i)}$ defined as

$$W^n_{(i)} = \left\{ r^n_{(i)}(x) = \sum_{k=-\infty}^{+\infty} d_{(i)}(k) \psi^n_b(2^{-i}x - k), \quad x \in \mathbb{R}, d_{(i)} \in l_2 \right\} \tag{3.7}$$

are such that

$$W^n_{(i+1)} \perp V^n_{(i+1)} \tag{3.8}$$

and

$$W^n_{(i+1)} \oplus V^n_{(i+1)} = V^n_{(i)}. \tag{3.9}$$

The first part of this theorem follows directly from (3.4). The last part is proved in Appendix A.

Since we know that (i) $\text{clos}_{L_2}(\bigcup_{i\in Z} V^n_{(i)}) = L_2$ and (ii) $\bigcap_{i\in Z} V^n_{(i)} = \{0\}$ [24], it follows from Theorem 1 that the set of functions $\{\psi^n_b(2^{-i}x-k)/\sqrt{2^i}, k\in\mathbb{Z}, i\in\mathbb{Z}\}$ is an unconditional basis of L_2. These results can also be generalized for modified wavelet functions obtained by linear combination (cf. (3.12)). These wavelets differ from those derived previously by Lemarié in that they are not orthogonal within the same resolution level, although they are constrained to be orthogonal between resolution levels.

Since $\beta^n(x)$ has compact support and that both $b^{2n+1}(k)$ and $u^n_2(k)$ are FIR operators, the wavelet ψ^n_b defined by (3.6) has compact support as well. The basic B-splines at resolution level (1) and their corresponding wavelets, as determined from (3.6), are shown in Fig. 1 for $n=1$ and 3. The wavelets are symmetric and shifted by one unit with respect to the standard B-spline functions. Note that the cubic B-spline is very similar to a Gaussian and that the corresponding wavelet resembles a modulated Gaussian (Gabor function). In fact, we have shown that the Gaussian approximation provided by this function improves for increasing order n [46].

3.2. Generalized polynomial spline wavelet transforms

To define a generalized polynomial spline wavelet transform with a given depth I (i.e., $i=1,\ldots,I$ where (i) is the resolution level), we consider two types of expansions. The first is the generic representation of a spline $g^n_{(i)}\in V^n_{(i)}$ at resolution level (i),

$$g^n_{(i)}(x) = \sum_{k=-\infty}^{+\infty} c_{(i)}(k)\varphi^n(2^{-i}x-k), \tag{3.10}$$

where the scaling function φ^n is defined by (2.2). The second is a representation of the corresponding residue $r^n_{(i)}\in W^n_{(i)}$,

$$r^n_{(i)}(x) = \sum_{k=-\infty}^{+\infty} d_{(i)}(k)\psi^n(2^{-i}x-k), \tag{3.11}$$

that uses a generalized spline wavelet

$$\psi^n(x) = \sum_{k=-\infty}^{+\infty} q(k)\psi^n_b(x-k), \tag{3.12}$$

where q is an invertible convolution operator from l_2 into itself. That the modified wavelets (3.12) form a basis of $W^n_{(i)}$ can be proved by the technique used in [47], Appendix A.

For a given signal $g^n_{(0)}$ initially represented by its polynomial spline coefficients at resolution (0), the use of (3.1) and Theorem 1 leads to the wavelet decomposition

$$g^n_{(0)}(x) = \sum_{k=-\infty}^{+\infty} c_{(0)}(k)\varphi^n(x-k) \tag{3.13a}$$

$$= \sum_{k=-\infty}^{+\infty} c_{(I)}(k)\varphi^n(2^{-I}x-k) + \sum_{i=1}^{I}\left(\sum_{k=-\infty}^{+\infty} d_{(i)}(k)\psi^n(2^{-i}x-k)\right), \tag{3.13b}$$

where the one-to-one linear mapping between the discrete signal coefficients in (3.13a) and (3.13b) is called the wavelet transform. The quantities $\{d_{(1)}, d_{(2)}, \ldots, d_{(I)}\}$ are the so-called wavelet coefficients; the sequence $\{c_{(I)}\}$, on the other hand, codes for the coarser resolution signal at resolution (I). This decomposition can in principle be carried out over all resolution levels and yields a representation equivalent to (1.1).

3.3. Biorthogonal splines and wavelets

To fully characterize this family of wavelet transforms, we also need a mechanism to determine the expansion coefficients in (3.13). For this purpose, we first derive a generalized sampling theorem which is an extension of a result initially reported in [45]. We will then show how the present

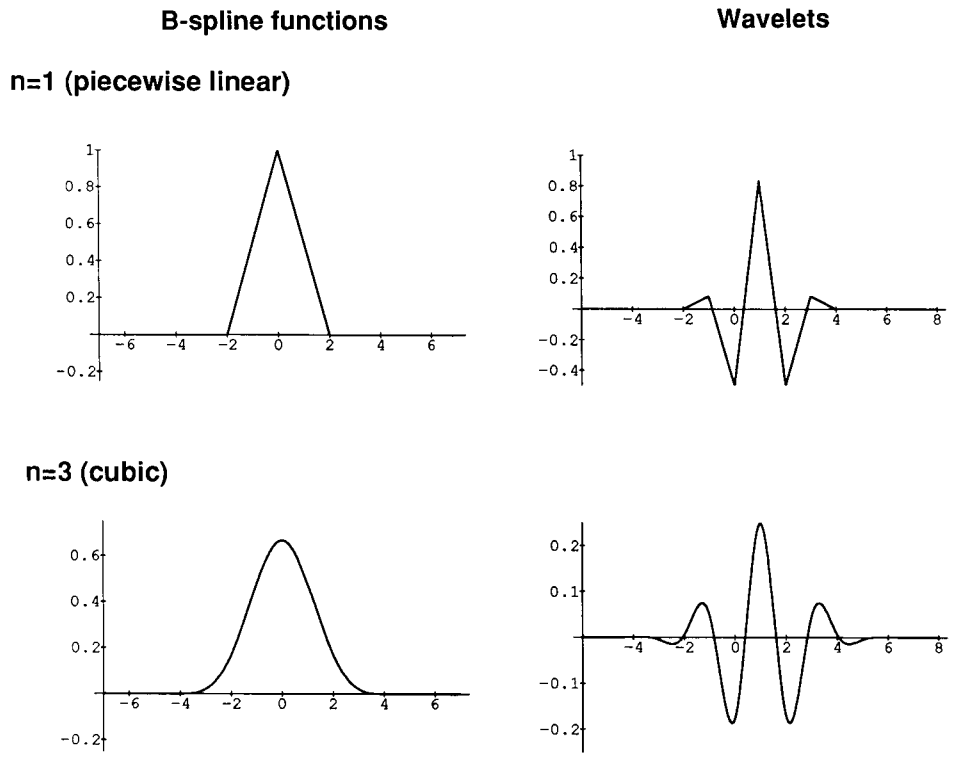

Fig. 1. Examples of B-spline scaling functions and wavelets at resolution level (1).

approach fits into the general theory of biorthogonal wavelet transforms [8, 19, 32, 50].

Consider an arbitrary basis function $\zeta(x)$ and the corresponding symmetrical discrete sequence

$$a(k)=\langle\zeta(x),\zeta(x-k)\rangle=\zeta'*\zeta(x)|_{x=k}, \quad (3.14)$$

where the notation $\zeta'(x)=\zeta(-x)$ stands for the time reversal of a function. We consider the associated function space V_m,

$$V_m=\Big\{g_m(x)=\sum_{k=-\infty}^{+\infty}c(k)\zeta_m(x-mk), \quad (x\in\mathbb{R},\ c(k)\in l_2)\Big\}, \quad (3.15)$$

where the basis functions are obtained by translation of the expanded kernel $\zeta_m(x)=\zeta(x/m)$. V_m is also assumed to be a closed subspace of L_2. A general procedure for determining the minimum error approximation of a function $g(x)$ in V_m is provided by the following theorem.

THEOREM 2. The expansion coefficients in (3.15) of the orthogonal projection of a function $g(x)\in L_2$ on V_m can be obtained by filtering and sampling,

$$c(k)=\frac{1}{m}\langle g(x),\mathring{\zeta}_m(x-mk)\rangle = \frac{1}{m}\mathring{\zeta}'_m * g(x)\Big|_{x=mk}, \quad (3.16)$$

where the dual function $\mathring{\zeta}_m(x)$ is given by

$$\mathring{\zeta}_m(x)=\sum_{k=-\infty}^{+\infty}(a)^{-1}(k)\zeta(x/m-k). \quad (3.17)$$

Note that the sequence $(a)^{-1}(k)$ must be well defined based on the well known property that the

orthogonal projection on a closed Hilbert space defines a bounded operator [20].

PROOF. We consider the case $m=1$. Since g_m is the orthogonal projection of g into V_m, the residual error must be orthogonal to the basis functions of V_m. Therefore, the coefficients $c(k)$ of the minimum error approximation must satisfy the relation

$$\langle g(x)-\sum_{k=-\infty}^{+\infty} c(l)\zeta(x-l), \zeta(x-k)\rangle=0 \quad \forall k\in\mathbb{Z}, \tag{3.18}$$

We now define the discrete sequence $u(k)$,

$$u(k)=\langle g(x), \zeta(x-k)\rangle=\zeta'*g(x)|_{x=k},$$

and note that

$$\left\langle \sum_{k=-\infty}^{+\infty} c(l)\zeta(x-l), \zeta(x-k)\right\rangle = a*c(k),$$

where the sequence $a(k)$ is defined by (3.14). With the use of these notations, (3.18) is also equivalent to

$$u(k)=a*c(k) \quad \forall k\in\mathbb{Z}.$$

Taking the convolution inverse of a, we find that

$$c(k)=(a)^{-1}*u(k)=\langle g(x), \mathring{\zeta}(x-k)\rangle,$$

where the function $\mathring{\zeta}(x)$ is given by

$$\mathring{\zeta}(x)=\sum_{k=-\infty}^{+\infty}(a)^{-1}(k)\zeta(x-k).$$

The general result is found by making a change of variable $x=y/m$ and applying the proper scaling to the sampled autocorrelation sequence. □

The role of $\mathring{\zeta}_m$ in (3.16) is analogous to that of an anti-aliasing filter used in conventional sampling theory [45]. From (3.17), we clearly have that $\mathring{\zeta}_m\in V_m$. Moreover, it is straightforward to show that the functions $\mathring{\zeta}_m$ and ζ_m are biorthogonal,

$$\langle \zeta_m(x-mk), \mathring{\zeta}_m(x-ml)\rangle=\begin{cases} m, & k=l,\\ 0, & \text{otherwise.}\end{cases} \tag{3.19}$$

Since we have made no restriction on the choice of ζ other than the fact that V_m is a closed subspace of L_2, we can apply this general result to obtain the expansion coefficients in the subspaces $V^n_{(i)}$ and $W^n_{(i)}$.

The autocorrelation sequence (3.14) for the *B*-spline scaling functions and wavelets are computed as follows:

$$\langle \beta^n(x), \beta^n(x-k)\rangle = b^{2n+1}(k), \tag{3.20}$$

$$\begin{aligned}\langle \psi^n_b(x), \psi^n_b(x-k)\rangle &= \tfrac{1}{2}[\underline{u}^n_2 * \underline{u}^n_2 * \underline{b}^{2n+1} * \underline{b}^{2n+1} * b^{2n+1}]_{\downarrow 2}(k)\\ &= b^{2n+1} * [\underline{b}^{2n+1} * b^{2n+1}]_{\downarrow 2}(k).\end{aligned} \tag{3.21}$$

Next, we use these results together with Theorem 2 to determine the dual functions associated with the generalized scaling functions and wavelets,

$$\mathring{\phi}^n(x)=\sum_{k=-\infty}^{+\infty}(p*p'*b^{2n+1})^{-1}(k)\beta^n(x-k), \tag{3.22}$$

$$\mathring{\psi}^n(x)=\sum_{k=-\infty}^{+\infty}(q*q'*b^{2n+1}*[\underline{b}^{2n+1}*b^{2n+1}]_{\downarrow 2})^{-1}(k) \times \psi^n_b(x-k). \tag{3.23}$$

These functions can be used to obtain the generalized spline expansion coefficients in (3.10) and (3.11) by using inner products, as indicated by (3.16) in Theorem 2. In particular, we can write the full wavelet expansion (1.1) as

$$g(x)=\sum_{i\in\mathbb{Z}}\sum_{k\in\mathbb{Z}}\frac{1}{2^i}\langle g(x), \mathring{\psi}^n(2^{-i}x-k)\rangle \times \psi^n(2^{-i}x-k), \tag{3.24}$$

a formula that is simple conceptually but not very efficient computationally. In the next section, we will show how to determine the expansion coefficients using an extension for non-orthogonal basis functions of Mallat's fast algorithm.

Some remarks concerning the properties of the present family of spline wavelets are in order. Since the corresponding residual spaces are also orthogonal to each other (cf. (3.2)), we have an even

stronger biorthogonality condition that holds over all resolution levels (i):

$$\langle \psi^n(2^{-i}x-k),\, \mathring{\psi}^n(2^{-j}x-l)\rangle = \begin{cases} 2^i, & i=j \text{ and } k=l, \\ 0, & \text{otherwise}, \end{cases} \tag{3.25}$$

which places the present approach in the more general framework of biorthogonal wavelet transforms. The basis functions $\mathring{\psi}^n(x)$ are the analysis wavelets associated with the synthesis wavelets $\psi^n(x)$. In the general biorthogonal scheme, the analysis and synthesis wavelet are different unless the basis functions are orthogonal [50]. Another point worth mentioning is that the wavelets in the general biorthogonal setting are usually not orthogonal across resolution levels which makes the orthogonal projection method described by Theorem 2 generally not suitable for determining the wavelet coefficients in the full expansion. In the general case, it is still possible to define biorthogonal wavelets pairs for obtaining the expansion coefficients, but these functions usually do not span the same approximation spaces [8]; this type of decomposition can also be interpreted in term of projections but the projectors are non-orthogonal, unlike in the present situation.

3.4. Fast wavelet transform algorithm

Since the function spaces $V^n_{(i)}$ are nested, the determination of the wavelet coefficients may proceed by repeated projection. This process can be accomplished efficiently by using the perfect reconstruction filter bank considered in Appendix A.

The starting point of such an analysis is a discrete signal $\{g(k)\}_{k\in\mathbb{Z}}$ which needs to be represented by a function $g(x)$ of the continuous variable x at the finer resolution level ($i=0$, by convention). A natural approach is to determine the coefficients of the polynomial spline that interpolates our sequence of data points. This interpolation problem can be solved efficiently by digital filtering [43]. In the present context, this leads to the initialization sequence

$$c_{(0)} = (p * b^n)^{-1} * g(k), \tag{3.26}$$

where the prefilter is the convolution inverse of the sequence $p * b^n(k)$, which depends on the particular choice of basis functions in (2.1).

The fast wavelet algorithm is then implemented by successive filtering and down-sampling by a factor of two,

$$c_{(i+1)}(k) := [\mathring{v} * c_{(i)}]_{\downarrow 2}(k), \tag{3.27}$$

$$d_{(i+1)}(k) := [\mathring{w} * c_{(i)}]_{\downarrow 2}(k), \tag{3.28}$$

where $\mathring{v}$ is given by (2.7), and where $\mathring{w}$ is defined as follows:

$$\mathring{w}(k) = \tfrac{1}{2}[(q * b^{2n+1})^{-1}]_{\uparrow 2} * p * \underset{\sim}{u}^n_2 * \delta_1(k). \tag{3.29}$$

These filter formulas correspond to the inverse z-transform of (A.9) and (A.10), respectively. This algorithm, which is described by the analysis part of the block diagram in Fig. 2, is applied iteratively for $i=0$ down to $I-1$, while retaining the wavelet coefficients for each level.

The reverse procedure, also implemented iteratively, is the re-synthesis of the finer resolution levels beginning with the coarsest level (bottom) of the pyramid. As shown in Appendix A, this algorithm can be implemented as follows:

$$c_{(i)}(k) = v * [c_{(i+1)}]_{\uparrow 2}(k) + w * [d_{(i+1)}]_{\uparrow 2}(k), \tag{3.30}$$

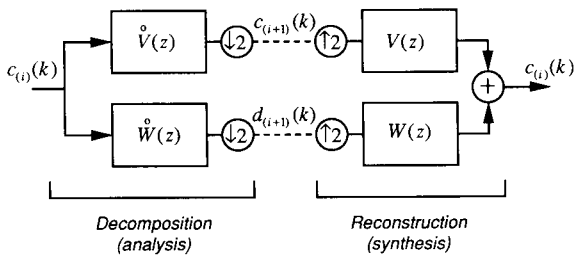

Fig. 2. Multirate filter bank for the evaluation of the direct and indirect wavelet transform.

where v is given by (2.10), and where w is defined as follows:

$$w(k) = \tfrac{1}{2}[q]_{\uparrow 2} * \underline{u}_2^n * \delta_{-1} * (p)^{-1}(k). \tag{3.31}$$

This procedure corresponds to the synthesis part in Fig. 2. Finally, our initial discrete signal $\{g(k)\}$ can be recovered by using the reverse of (3.26), which provides a sampling of $g_{(0)}^n(x)$ at the integers,

$$g(k) = p * b^n * c_0(k). \tag{3.32}$$

The full procedure is an extension of Mallat's fast wavelet algorithm for non-orthogonal basis functions. The present approach is general in the sense that it is valid for any choice of the parameters p and q. A way of fixing those operators is to impose certain desirable properties on the basis functions (cf. Section 4.1).

Our derivation of the wavelet algorithm in Appendix A uses a set of conditions (A.10) that are well known in multirate filter bank theory [48, 49]. These conditions are necessary and sufficient for a perfect reconstruction. In other words, they guarantee the reversibility of the filter bank algorithm. A less well known result, which is derived in Appendix B, is that this property can also be expressed by the following set of equations:

$$[\mathring{v} * v]_{\downarrow 2}(k) = \langle \mathring{v}'(l), v(l+2k)\rangle_{l_2} = \delta_0(k), \tag{3.33a}$$

$$[\mathring{w} * w]_{\downarrow 2}(k) = \langle \mathring{w}'(l), w(l+2k)\rangle_{l_2} = \delta_0(k), \tag{3.33c}$$

$$[\mathring{w} * v]_{\downarrow 2}(k) = \langle \mathring{w}'(l), v(l+2k)\rangle_{l_2} = 0, \tag{3.33c}$$

$$[\mathring{v} * w]_{\downarrow 2}(k) = \langle \mathring{v}'(l), w(l+2k)\rangle_{l_2} = 0, \tag{3.33d}$$

where $\langle \cdot, \cdot \rangle_{l_2}$ denotes the standard l_2-inner product. Equations (3.33a–d) are quite general and must be satisfied for any orthogonal or biorthogonal wavelet algorithm (cf. [32], for the special case of a FIR/FIR filter bank). They can be interpreted as discrete biorthogonality ((a) and (b)) and orthogonality ((c) and (d)) conditions on the impulse responses. Equations (3.33a) and (3.33b) also provide a justification of our use of the biorthogonality symbol '°' to represent the analysis filters.

3.5. Extension in higher dimensions

These results can be readily extended to higher dimensions through the use of tensor product splines [31, 37]. In two dimensions, there are four distinct types of basis functions corresponding to the different cross-products of one-dimensional spline scaling functions and wavelets:

$$\begin{aligned} \varphi^n(x, y) &= \varphi^n(x)\varphi^n(y), \\ \psi_x^n(x, y) &= \psi^n(x)\varphi^n(y), \\ \psi_y^n(x, y) &= \varphi^n(x)\psi^n(y), \\ \psi_{xy}^n(x, y) &= \psi^n(x)\psi^n(y). \end{aligned} \tag{3.34}$$

The corresponding 2D wavelet transform is separable. Hence, a 2D spline wavelet transform can be obtained by successive one-dimensional wavelet transformation along the rows and columns. A mathematical justification for this type of approach can be found in [25].

4. Specific wavelet representations

A suitable selection of the convolution operators p and q in (2.2) and (3.12) allows the construction of a variety of polynomial spline wavelets with certain specific properties. We have identified four representations that are the logical complements of the polynomial spline representations considered in [47]. The main properties of these wavelet transforms are summarized in Table 2. Examples of cubic spline wavelets ($n=3$) are shown in Fig. 3.

4.1. Orthogonal Lemarié–Battle wavelet transform (O-splines)

The polynomial spline wavelet transforms decribed in previous studies use orthogonal basis functions [3, 21]. It can be verified that imposing such an orthogonality constraint leads to the following weighting sequences:

$$\begin{aligned} p_o &= (b^{2n+1})^{-1/2}, \\ q_o &= ([\underline{b}^{2n+1} * b^{2n+1}]_{\downarrow 2} * b^{2n+1})^{-1/2}, \end{aligned} \tag{4.1}$$

and that the corresponding spline and wavelet basis

Table 2
Alternative sets of spline and wavelet basis functns and their specific properties

	Orthogonal (*O*-splines)	Basic (*B*-splines)	Cardinal (*C*-splines)	Dual (*D*-splines)
Specific properties	Orthogonality	Compact support fast EXPAND good localization	Interpolation	Fast REDUCE
Basic function	φ_o^n	$\varphi_b^n = \beta^n$	φ_c^n	$\varphi_d^n = \tilde{\varphi}_b^n$
Weighting coefficients (p)	$(b^{2n+1})^{-1/2}$	δ_0	$(b^n)^{-1}$	$(b^{2n+1})^{-1}$
Wavelet functions	ψ_o^n	ψ_b^n	ψ_c^n	$\psi_d^n = \tilde{\psi}_b^n$
Weighting coefficients (p)	$(b^{2n+1} * [\underline{b}^{2n+1} * b^{2n+1}]_{\downarrow 2})^{-1/2}$	$\delta_0(k)$	$([b^n * \underline{u}_2^n * \underline{b}^{2n+1}]_{\downarrow 2})^{-1}$	$(b^{2n+1} * [\underline{b}^{2n+1} * b^{2n+1}]_{\downarrow 2})^{-1}$

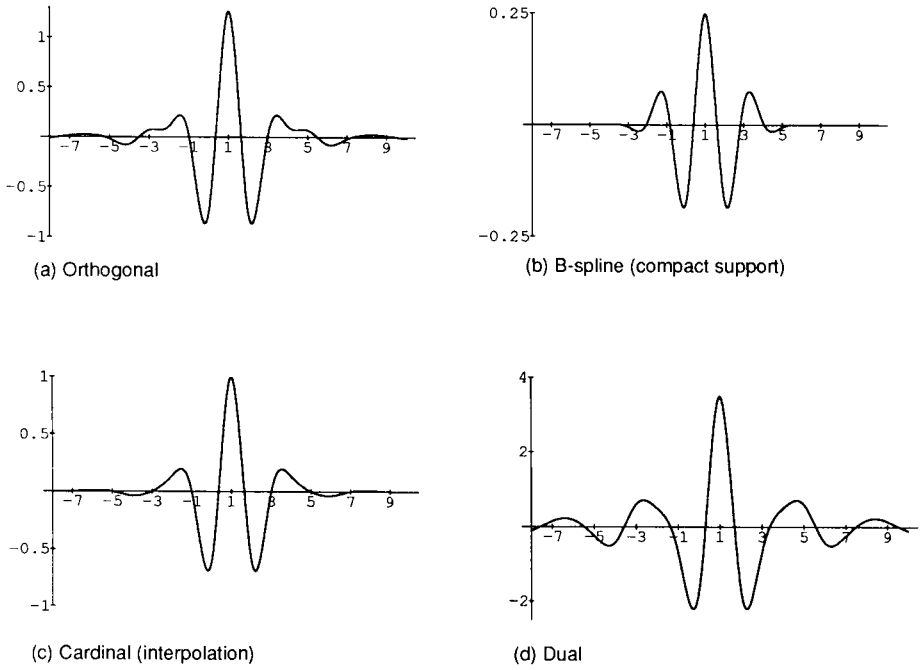

Fig. 3. Examples of cubic spline wavelets at resolution level (1).

functions are identical to those described in [21]. The main advantage of the orthogonal representation is that the analysis and synthesis filters are identical and can all be obtained from a single prototype:

$$v_o = \tfrac{1}{2}[(b^{2n+1})^{-1/2}]_{\downarrow 2} * (b^{2n+1})^{1/2} * u_2^n.$$

This property is also valid in the case of a general wavelet transform [50]. It can be verified by substitution of (4.1) in (3.29) that the corresponding

wavelet filter is the conjugate (or quadrature mirror) filter: $w_o = \delta_1 * \underline{v}_o$, in agreement with Mallat's general results for the orthogonal wavelet transform.

4.2. Wavelet transform of compact support (B-splines)

In the present formulation, the most obvious choice is $p = q = \delta_0$, in which case the polynomial spline and wavelet basis functions all have a compact support. This particular case also corresponds to the wavelet transform described by Chui and Wang, with the slight difference that their basis functions are shifted with respect to ours [7]. The choice of this representation tends to simplify the reconstruction process (indirect wavelet transform) as the corresponding filters are binomial or modulated binomial FIR kernels. Moreover, the decomposition filters have a simple recursive structure and can be implemented efficiently using a technique similar to the one described in [43]; this point is further elaborated in Section 4.5.

What also makes these functions particularly attractive is their excellent time–frequency localization. In fact, we proved that the *B*-spline wavelets tend to Gabor functions as the order of the spline n goes to infinity [46]. These latter functions are modulated Gaussians; they are known to be optimal with respect to the uncertainty principle (i.e. maximum energy concentration in both the time and the frequency domain) [15]. The quality of the Gabor approximaton is surprisingly good, even for small values of n. For instance, for $n = 3$, the relative L_2 approximation error is 2.6% and the product of the time–frequency uncertainties for the cubic *B*-spline wavelet is within 2% of the limit specified by the uncertainty principle. These good localization properties and the availability of fast algorithms should make the *B*-spline wavelet transform useful for the analysis of non-stationary signals.

4.3. Cardinal wavelet transform (C-splines)

Another possibility is to construct wavelets for which the coefficients are the sample values of the residual signal. These basis functions must satisfy the interpolation condition

$$\psi_c^n(k + \tfrac{1}{2}) = \begin{cases} 1, & \text{if } k = 0, \\ 0, & \text{if } k \neq 0 \end{cases} \quad \forall k \in \mathbb{Z}. \tag{4.2}$$

This is the wavelet counterpart of the cardinal or fundamental spline representation [43], which has the convolution operator

$$p_c = (b^n)^{-1}.$$

Condition (4.2) translates into a constraint on the reconstruction filter,

$$[\delta_{-1} * w]_{\downarrow 2}(k) = q_c * [b^n * \underline{u}_2^n * \underline{b}^{2n+1}]_{\downarrow 2}(k) = \delta_0(k). \tag{4.3}$$

By solving this equation, we find the cardinal weighting sequence

$$q_c = ([b^n * \underline{u}_2^n * \underline{b}^{2n+1}]_{\downarrow 2})^{-1}. \tag{4.4}$$

The corresponding cardinal spline/wavelet decomposition allows a better visualization of the underlying continuous signals because the expansion coefficients are the sample values of the coarser resolution spline and wavelet signal components. Furthermore, the computational complexity of the reconstruction algorithm can be halved; it is only necessary to compute the finer resolution coefficients between knot points (interpolation). It can be seen from Fig. 3 that the cardinal and orthogonal cubic spline wavelet functions are quite similar. The essential difference, however, is that the former basis functions are precisely equal to one for $x = 1$ (center of symmetry) and vanish for all other odd-valued indices.

4.4. Dual wavelet transform (D-splines)

Another interesting case is to try simplifying the structure of the analysis filters as much as possible. This leads to the dual spline representation with

$$\begin{aligned} p_d &= (b^{2n+1})^{-1}, \\ q_d &= ([\underline{b}^{2n+1} * b^{2n+1}]_{\downarrow 2} * b^{2n+1})^{-1}, \end{aligned} \tag{4.5}$$

with precisely the same filters as the *B*-spline wavelet transform but in reverse order. This situation

corresponds to a flow graph transposed version of the B-spline case. These dual wavelets are denoted by ψ_{d}^n. They are indeed the dual of the B-spline wavelets in the sense that they satisfy the biorthogonality condition (3.25); i.e., $\psi_{\mathrm{d}}^n = \mathring{\psi}_{\mathrm{b}}^n$. This also means that the dual spline wavelet is the analysis wavelet associated with the B-spline representation, and vice versa (cf. Section 3.3). A different – but equivalent – definition of these particular functions is also given in [7].

4.5. Implementation

The digital filters for the fast wavelet algorithm for all these cases can be obtained from (2.7), (2.10), (3.29) and (3.31) by substitution of the corresponding expressions for p and q. General formulas for the transfer functions of these filters are given in Table 3. These results are illustrated in Fig. 4 with the frequency responses of the analysis filter bank for $n=3$ (cubic splines).

Although the filter bank implementation appears to be relatively straightforward, there are several practical issues that need to be dealt with. These are briefly discussed below.

4.5.1. Choice of the finer resolution signal model

In signal and image processing applications, our initial data representation is a sequence (or array) of sample values $g(k)$. Our approach to choosing the initial signal model is to determine the polynomial spline that interpolates $g(k)$. By convention, the initial step size is assumed to be one. Based on the results in Section 3.4, the initial spline coefficients at level (0) are obtained by convolution (prefilter) using (3.26). The frequency responses of the corresponding filters for cubic splines are represented by dotted lines in Fig. 4. The advantage of using such an initialization procedure is that our initial signal model is uniquely defined and is independent of our choice of basis functions. Likewise, we can apply the inverse procedure (3.32) to reconstruct the digital signal from its finer resolution spline coefficients. Note that the use of such filters is not necessary in the cardinal representation ($p=(b^n)^{-1}$).

4.5.2. Boundary conditions

Since the signals or sequences encountered in practice have a finite extent: $\{c_{(0)}(k),\ k=1,\ldots,K_0\}$, we have to introduce some boundary conditions. A consistent implementation of these boundary conditions is important to guarantee that the wavelet transform is fully reversible. For practical convenience and to avoid discontinuities, we have chosen to extend the signal on both sides by using its mirror image, a standard practice in image

Table 3
Frequency responses of the filters for the evaluation of polynomial spline wavelets

Representation	$\mathring{V}(f)$	$V(f)$	$e^{j2\pi f}\mathring{W}$	$e^{-j2\pi f}W(f)$
General	$\frac{1}{2}\frac{U_2^n(f)B_1^{2n+1}(f)P(f)}{B_1^{2n+1}(2f)P(2f)}$	$\frac{U_2^n(f)P(2f)}{P(f)}$	$\frac{1}{2}\frac{U_2^n(f+\frac{1}{2})P(f)}{B_1^{2n+1}(2f)Q(2f)}$	$\frac{U_2^n(f+\frac{1}{2})B_1^{2n+1}(f+\frac{1}{2})Q(2f)}{P(f)}$
Orthogonal	$\frac{1}{2}U_2^n(f)\sqrt{\frac{B_1^{2n+1}(f)}{B_1^{2n+1}(2f)}}$	$U_2^n(f)\sqrt{\frac{B_1^{2n+1}(f)}{B_1^{2n+1}(2f)}}$	$\frac{1}{2}U_2^n(f+\frac{1}{2})\sqrt{\frac{B_1^{2n+1}(f+\frac{1}{2})}{B_1^{2n+1}(2f)}}$	$U_2^n(f+\frac{1}{2})\sqrt{\frac{B_1^{2n+1}(f+\frac{1}{2})}{B_1^{2n+1}(2f)}}$
Basic	$U_2^n(f)\left(\frac{B_1^{2n+1}(f)}{B_1^{2n+1}(2f)}\right)$	$U_2^n(f)$	$\frac{1}{2}\frac{U_2^n(f+\frac{1}{2})}{B_1^{2n+1}(2f)}$	$U_2^n(f+\frac{1}{2})B_1^{2n+1}(f+\frac{1}{2})$
Cardinal	$\frac{1}{2}U_2^n(f)\left(\frac{B_1^n(2f)B_1^{2n+1}(f)}{B_1^n(f)B_1^{2n+1}(2f)}\right)$	$U_2^n(f)\left(\frac{B_1^n(f)}{B_1^n(2f)}\right)$	$\frac{1}{2}\frac{U_2^n(f)C^n(f)B_1^{2n+1}(f+\frac{1}{2})}{B_1^n(f)B_1^{2n+1}(2f)}$	$\frac{U_2^n(f+\frac{1}{2})B_1^n(f)B_1^{2n+1}(f+\frac{1}{2})}{C^n(f)}$
Dual	$\frac{1}{2}U_2^n(f)$	$U_2^n(f)\left(\frac{B_1^{2n+1}(f)}{B_1^{2n+1}(2f)}\right)$	$\frac{1}{2}U_2^n(f+\frac{1}{2})B_1^{2n+1}(f+\frac{1}{2})$	$\frac{U_2^n(f+\frac{1}{2})}{B_1^{2n+1}(2f)}$

Where $U_2^n(f)=2\cos^{n+1}(\pi f)$, $B_1^n(f)=\sum_{k=-\infty}^{+\infty}[\mathrm{sinc}(f-k)]^{n+1}=b^n(0)+\sum_{k=1}^{(n+1)/2}2b^n(k)\cos(2\pi kf)$ and $C^n(f)=\frac{1}{2}(U_2^n(f+\frac{1}{2})B_1^n(f)B_1^{2n+1}(f+\frac{1}{2})+U_2^n(f)B_1^n(f+\frac{1}{2})B_1^{2n+1}(f))$.

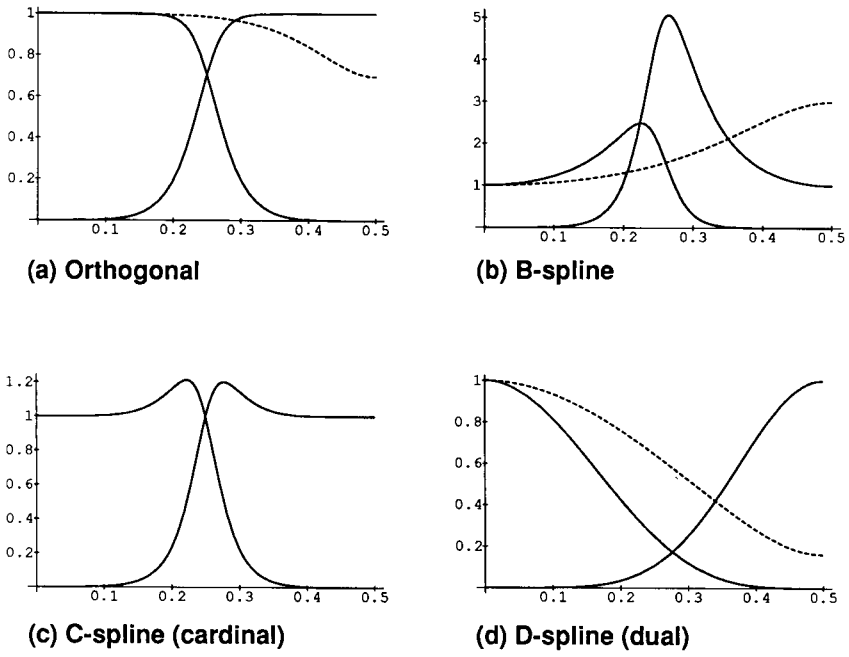

Fig. 4. Transfer functions of the analysis filters ($\mathring{V}(f)$ and $\mathring{W}(f)$) for various cubic spline wavelet transforms. The highpass filter extracts the wavelet components, while the lowpass filter produces a lower resolution signal approximation. The graph in dotted lines represents the frequency response of the prefilter that converts the initial signal values (cardinal representation) to the corresponding spline representation.

processing. In specifying such boundary conditions, one has to distinguish between whether one performs a signal decomposition or a reconstruction from its lower resolution coefficients. In each case, we will assume that the size of the signal at the finer resolution level is twice that at the next coarser one, which sets the constraints: $K_{(i)}$ even and $K_{(0)} = K_{(I)} 2^I$, where $K_{(i)}$ is the number of spline or wavelet coefficients at level (i) and I the depth of the decomposition. For the direct wavelet transform (downward direction), the boundary conditions on the input sequence are

$$\begin{aligned} &c_{(i)}(-k) = c_{(i)}(k+2), \\ &\quad k = 0, \ldots, K_{(i)} - 1, \\ &c_{(i)}(k) = c_{(i)}(2K_{(i)} - k), \\ &\quad k = K_{(i)}, \ldots, 2K_{(i)} - 1. \end{aligned} \tag{4.6}$$

It can be verified that the compatible boundary conditions for the indirect wavelet transform (upward direction) are

$$\begin{aligned} &c_{(i+1)}(-k) = c_{(i+1)}(k+2), \\ &\quad k = 0, \ldots, K_{(i+1)} - 1, \\ &c_{(i+1)}(k) = c_{(i+1)}(K_{(i)} - k + 1), \\ &\quad k = K_{(i+1)}, \ldots, K_{(i)} - 1; \end{aligned} \tag{4.7}$$

$$\begin{aligned} &d_{(i+1)}(-k) = d_{(i+1)}(k+1), \\ &\quad k = 0, \ldots, K_{(i+1)} - 1, \\ &d_{(i+1)}(k) = d_{(i+1)}(K_{(i)} - k), \\ &\quad k = K_{(i+1)}, \ldots, K_{(i)} - 1, \end{aligned} \tag{4.8}$$

where $K_{(i)} = 2K_{(i+1)}$ is even.

4.5.3. Recursive implementation

It has been mentioned that the IIR filters that appear in the basic, cardinal or dual wavelet transform can be implemented recursively. To illustrate this principle, we consider the evaluation of the

wavelet coefficients in the basic representation ($p_b = q_b = \delta_0$),

$$d_{(i+1)}(k) = \left[\tfrac{1}{2}[(b^{2n+1})^{-1}]_{\downarrow 2} * \underline{u}_2^n * c_{(i)}\right]_{\downarrow 2}(k)$$
$$= (b^{2n+1})^{-1} * \left[\tfrac{1}{2}\underline{u}_2^n * c_{(i)}\right]_{\downarrow 2}(k), \qquad (4.9)$$

which can be evaluated in two steps. The first is to perform a FIR prefiltering with $\frac{1}{2}\underline{u}_2^n$ while downsampling by a factor of two. The second is to apply the postfilter $(b^{2n+1})^{-1}$ which corresponds to a direct B-spline transform of order $2n+1$ [43]. This filter can be implemented very efficiently by decomposing it into a product of first order causal and anticausal recursive filters with a total complexity of approximately $2n$ additions and $2n$ multiplications per sample points. A similar procedure is applicable for the implementation all other IIR in the basic, cardinal and dual representations.

4.5.4. *FIR approximations*

The other approach is to use a truncated FIR approximation. This technique has the advantage of simplicity but introduces approximation errors. The simplest design method is to evaluate the frequency response of a given filter using the formulas in Table 3 and to perform an inverse FFT transform to obtain the coefficients of the impulse response. The impulse response is then truncated to an appropriate length to satisfy a prescribed tolerance error. We note that this technique is the only one applicable for the implementation of the orthogonal transformation.

5. Results and discussion

5.1. *Image processing examples*

We illustrate the above with some examples. Our 256×256 test image (Fig. 5(a)) is a combination of two Brodatz textures (wood and sand) after intensity scale normalization [4]. This example was selected to test the usefulness of the wavelet transform for texture analysis and segmentation. We used a separable implementation in which the 2D wavelet coefficients were determined by successive filtering and decimation along the rows and columns of an image.

The cubic C-spline wavelet transform with a depth of two is shown in Fig. 5(b); each wavelet sub-image has had its gray scale linearly expanded for maximum contrast display. Note that the wavelet components in the upper right (V), lower left (H) and lower right (D) quadrants tend to amplify high resolution vertical, horizontal and diagonal edges, respectively. The two texture regions can be differentiated on the basis of their relative energy contribution to the different channels of the decomposition. Wood texture contributes little to the horizontal (H and h) and diagonal (D and d) channels; but both vertical channels (V and v) are enhanced because of the strong directionality of the underlying structure. Figure 6(a) displays the corresponding image coefficients of the orthogonal polynomial spline functions obtained by filtering Fig. 5(a). Although the conversion filter attenuates higher frequencies slightly (cf. Fig. 4(a)), the images in Figs. 6(a) and 5(a) are virtually indistinguishable; the same is true for the orthogonal and cardinal cubic spline wavelet transforms (cf. Figs. 5(b) and 6(b)). The cubic spline coefficients of the image in Fig. 5(a) and the corresponding B-spline wavelet coefficients are displayed in Figs. 7(a) and 7(b), respectively. Both appear to be visually sharper than their counterparts in Fig. 5. Finally, Fig. 8 displays the dual cubic spline coefficients (Fig. 8(a)) and the corresponding D-spline wavelet transform (Fig. 8(b)) which both appear to be smoother.

5.2. *Discussion*

These different types of wavelet decomposition are all equivalent but they exhibit distinct properties. We will now present arguments to facilitate the choice of a transform appropriate to a specific application.

The main advantage of the orthogonal representation is that the l_2-norm in the transform domain is equivalent to the L_2-norm in the continuous signal domain. This is especially relevant in coding

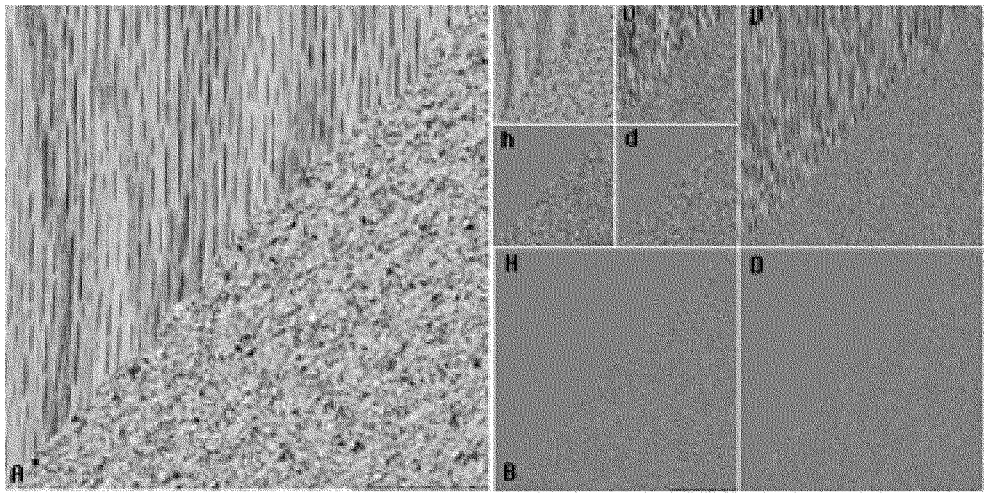

Fig. 5. Two-dimensional cardinal cubic spline wavelet transform. (a) Original texture composite; (b) *C*-spline wavelet transform.

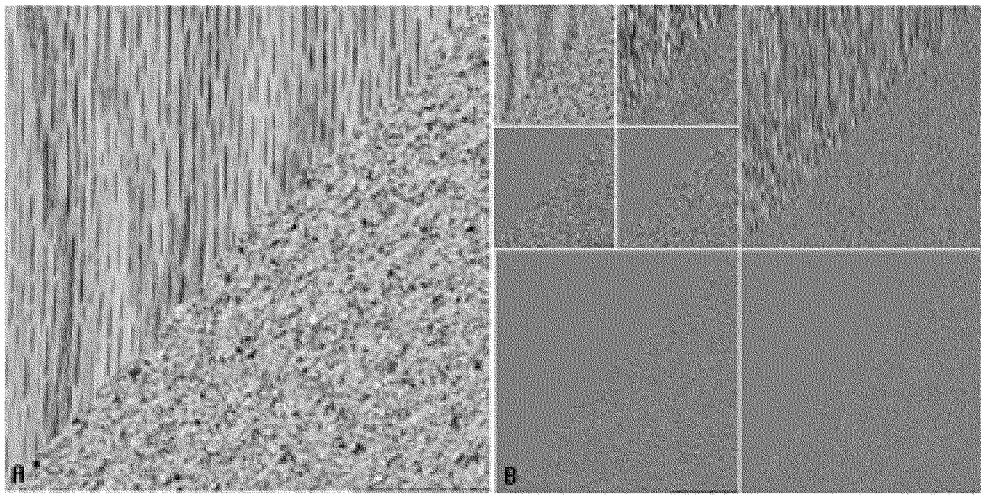

Fig. 6. Two-dimensional orthogonal cubic spline wavelet transform. (a) Orthogonal spline coefficients; (b) *O*-spline wavelet transform.

applications, see for example [1, 25, 38]. The correspondence between approximation errors in the signal and transform domain justifies the use of LMS error criteria for encoding the wavelet coefficients. Examples of such schemes are the Lloyd–Max quantizer [28], and vector quantization [16, 17, 22], a multivariate extension of the former. To illustrate the optimality of the orthogonal representation with respect to an LMS coding strategy, we have constructed an experiment using two test images: the standard 'Lena' image and the texture composite in Fig. 5(a). We applied a minimum error quantizer to the wavelet coefficients in the first three quadrants of the various cubic spline wavelet transforms, while the lower resolution components were coded with no error. The results are summarized in Table 4 in terms of the signal-to-noise ratio (dB) between the

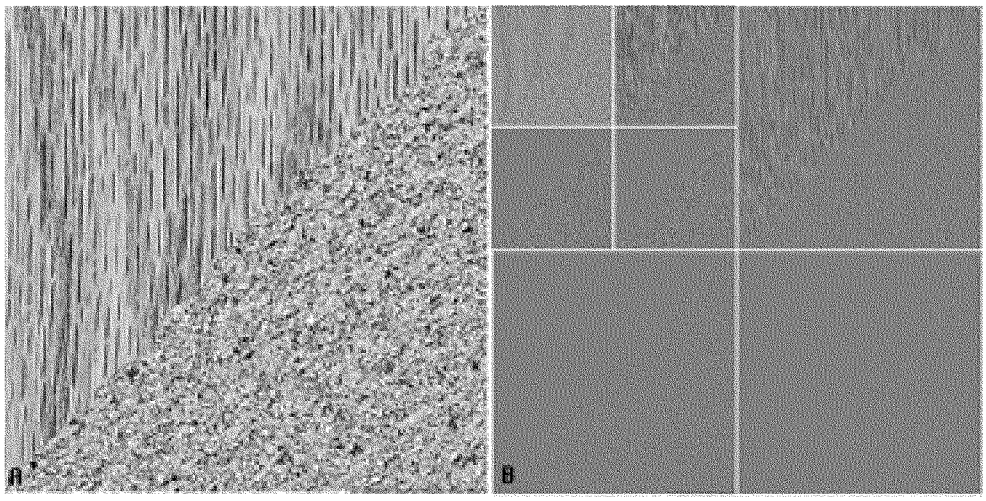

Fig. 7. Two-dimensional cubic *B*-spline wavelet transform. (a) Cubic *B*-spline coefficients; (b) *B*-spline wavelet transform.

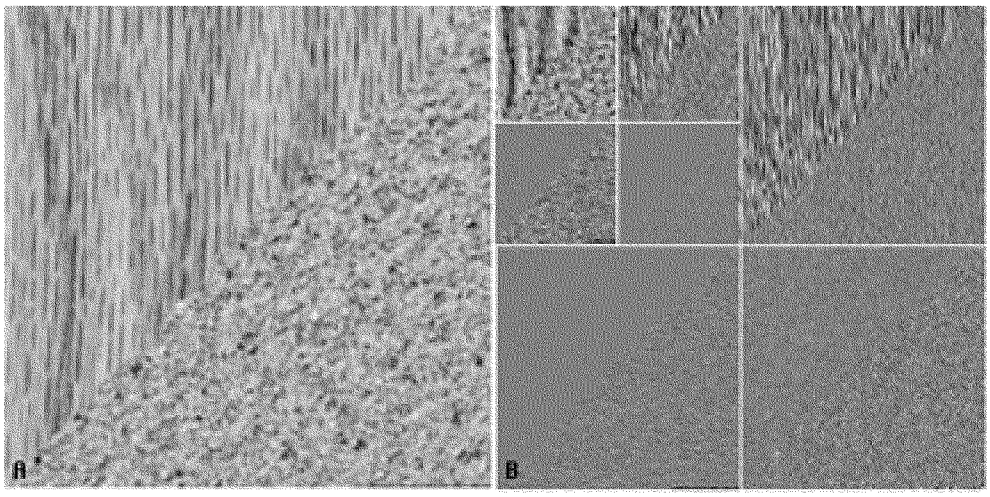

Fig. 8. Two-dimensional dual cubic spline wavelet transform. (a) Cubic *B*-spline coefficients; (b) *D*-spline wavelet transform.

Table 4

Signal-to-noise ratios resulting from the quantification of the coefficients in the first level of various cubic spline wavelet transforms

Quantification levels	*O*-splines	*B*-splines	*C*-splines	*D*-splines
'Lena' image				
$n_q = 3$	33,23 dB	25.52 dB	32.44 dB	29.29 dB
$n_q = 7$	36.96 dB	27.80 dB	35.89 dB	31.81 dB
Texture composite				
$n_q = 3$	28.17 dB	21.91 dB	27.92 dB	21.10 dB
$n_q = 7$	33.92 dB	25.77 dB	33.67 dB	25.21 dB

various approximations and the original image. Not surprisingly, the *O*-spline representation outperforms the *B*-splines and *D*-spline wavelet transforms. The *C*-spline representation, on the other hand, is only slightly sub-optimal.

The cardinal representation is well suited for conventional signal processing for it provides a precise rendition of the underlying continuous functions in terms of sampled values. It requires no pre-filter, otherwise necessary for consistent representation of a discrete sequence by polynomial splines. In practice, the distinction between this representation and the *O*-spline decomposition is usually quite subtle (cf. Figs. 5 and 6, as well as Table 4). The cardinal spline wavelet should therefore also be a good candidate for coding. A practical advantage of the latter could be to reduce decoding complexity (i.e., one half of the synthesis filter coefficients are zero so that only every other term has to be evaluated).

The *B*-spline wavelets can be closely approximated by Gabor functions [46]. They are therefore very well localized in space (or time) and frequency. The *B*-spline wavelet transform is in this sense very similar to the hierarchical Gabor decomposition designed empirically by Daugman using neural networks [11]. A clear advantage of the wavelet transform is the orthogonality of the basis functions between resolution levels and the availability of fast algorithms. Because of these properties, the *B*-spline wavelet transform also appears to be especially suited for the analysis of non-stationary signals [14].

Another feature of the *B*-spline representation is the compact support of the basis functions. This property could be especially useful for performing numerical computations with a high degree of precison since no truncation of the basis functions is required. It may also be a significant advantage in the design of finite element methods for the numerical solution of differential equations. This property will translate into systems of equations that are band-diagonal and can be solved very efficiently by gaussian elimination or LU factorization. In terms of numerical stability and ease of computation, the spline wavelets of compact support appear to offer the same advantages as the classical *B*-spline functions used routinely in a variety of engineering and applied mathematics applications [12, 31].

The main advantage of the dual representation is the simplicity of the analysis filters (simple FIR kernels); this may be an asset in some pattern recognition applications. This technique could for example be useful for texture segmentation using a multi-resolution extension of the method described in [44]. There is also a direct link between this representation and a number of earlier multiresolution techniques such as scale-space filtering [23, 51] and the Gaussian pyramid [5, 6]; this issue is further discussed in [47].

The analysis wavelets for the dual decomposition are the *B*-spline wavelets, which are very similar to Gabor functions. Based on this observation, certain parallels can be made with our current understanding of the way in which the human visual system operates. For instance, Gabor functions have been shown to provide good models for the receptive fields of simple cortical cells; the hierarchical organization of the visual cortex is also well documented [13, 26]. In fact, this type of arguments has been the basis for many applications of the Gabor transform in image processing, mainly for texture segmentation [30, 42].

We have already pointed out the similarity between the orthogonal and cardinal spline representations. In fact, this resemblance improves as the order of the spline is increased. Moreover, we have the following asymptotic relations:

$$\lim_{n\to\infty} \varphi_c^n(x) = \lim_{n\to\infty} \tilde{\varphi}_c^n(x) = \lim_{n\to\infty} \varphi_o^n(x) = \operatorname{sinc}(x), \tag{5.1}$$

$$\lim_{n\to\infty} \psi_c^n(x) = \lim_{n\to\infty} \tilde{\psi}_c^n(x) = \lim_{n\to\infty} \psi_o^n(x) = \cos\left(\frac{3\pi(x-1)}{2}\right) \operatorname{sinc}\left(\frac{x-1}{2}\right), \tag{5.2}$$

where $\operatorname{sinc}(x) := \sin(\pi x)/\pi x$. An implication is that the corresponding wavelet analysis and synthesis filters tend to the ideal discrete lowpass and highpass filters as the order of the spline goes to infinity.

Hence, the bandpass characteristics of the filter bank tend to improve for higher order splines. The polynomial spline wavelet transform is therefore in essence a subband signal decomposition. Lemarié has proven the pointwise convergence of the frequency response of $\psi_o^n(x)$ to the ideal highpass filter [21]. Different aspects of the convergence of $\varphi_c^n(x)$ to $\mathrm{sinc}(x)$ are discussed in [2, 27, 36]. These include convergence in the L_p-norm, which has also been shown to hold for $\mathring{\varphi}_c^n(x)$ and $\varphi_o^n(x)$[45]; the same ideas can be used to construct a proof for the convergence of $\psi_c^n(x)$, $\mathring{\psi}_c^n(x)$ and $\psi_o^n(x)$. For the reader unfamiliar with these concepts, we recall that L_p-norm convergence is a much stronger result than pointwise convergence. Pointwise convergence in the frequency domain alone does not imply convergence of the basis functions themselves. The L_p-norm convergence, on the other hand, has an interpretation in both time and frequency domain. For instance, it is well known that the norm of the difference for $p=2$ is identical in both domains (Parseval's identity).

6. Conclusion

In this paper, we have extended the construction of the polynomial spline wavelet transform initially proposed by Lemarié and Battle by relaxing the orthogonality condition of the wavelet basis functions. In particular, we have described polynomial spline wavelets of compact support which are the natural counterpart of the standard B-splines. An interesting feature of these wavelets is their excellent time–frequency localization, a property that is especially relevant for the analysis of non-stationary signals. Other related basis functions have been generated by reversible translation-invariant linear transformations. We have also shown how to extend Mallat's fast decomposition (respectively reconstruction) algorithm, which operates by iterated filtering and decimation (respectively up-sampling and post-filtering), for the evaluation of the class of polynomial spline wavelet transforms. The corresponding analysis and synthesis filters are not necessarily identical but can take a simple form (e.g. FIR binomial filters). Using simplified FIR or recursive filter structures may reduce computational complexity as well as improve numerical precision and stability.

We have emphasized the cardinal spline wavelet transform; the sole wavelet in this family to provide a signal decomposition in terms of the sample values of the underlying continuous functions. The corresponding basis functions are true interpolaton kernels and are in this sense very similar to sinc or modulated-sinc functions. An interesting feature of this class of wavelet transforms is to include two important limit cases: for $n=0$, we have a decomposition using piecewise constant functions (Haar transform), while as n tends to infinity the wavelet transform becomes the classical subband decomposition of a signal using ideal lowpass and highpass filters. For intermediate values of n (e.g., $n=3$), the filter banks associated with the orthogonal or cardinal spline wavelet decomposition have good bandpass characteristics which should make them useful in a number of applications.

Appendix A. Proof of Theorem 1

In the proof, we will represent splines using the generalized scaling functions and wavelets discussed in Section 3.2. The situation described in Theorem 1 corresponds to the particular case $p=q=\delta_0$. Equation (3.3) implies that $W_{(i+1)}^n \subset V_{(i)}^n$. Moreover, the orthogonality property of $\psi_b^n(x)$ implies that $W_{(i+1)}^n \perp V_{(i+1)}^n$. To prove that $W_{(i+1)}^n \oplus V_{(i+1)}^n = V_{(i)}^n$, we will show that any function $g_{(i)}^n \in V_{(i)}^n$ can be expressed as a linear combination of basis functions of $W_{(i+1)}^n$ and $V_{(i+1)}^n$,

$$\begin{aligned} g_{(i)}^n(x) &= \sum_{k=-\infty}^{+\infty} c_{(i)}(k)\varphi^n(2^{-i}x-k) \\ &= \sum_{k=-\infty}^{+\infty} c_{(i+1)}(k)\varphi^n(2^{-(i+1)}x-k) \\ &\quad + \sum_{k=-\infty}^{+\infty} d_{(i+1)}(k)\psi^n(2^{-(i+1)}x-k), \end{aligned} \tag{A.1}$$

where φ^n and ψ^n are defined by (2.2) and (3.29), respectively. We start by expressing the coarser grid basis functions in terms of the scaling function on the finer grid. By using (2.4), (3.3) and performing the appropriate change of coordinates, we find that

$$\varphi^n(x/2)=\sum_{k=-\infty}^{+\infty} v(k)\varphi^n(x-k), \tag{A.2}$$

$$\psi^n(x/2)=\sum_{k=-\infty}^{+\infty} w(k)\varphi^n(x-k), \tag{A.3}$$

where the sequences v and w are given by (2.10) and (3.31), respectively. A direct implication is that the coefficients $c_{(i)}$ can be recovered from the coarser level coefficients $c_{(i+1)}$ and $d_{(i+1)}$ using the procedure schematized in the right part of Fig. 2. The transfer function of the corresponding synthesis filters are

$$V(z)=\frac{U_2^n(z)P(z^2)}{P(z)}, \tag{A.4}$$

$$W(z)=\frac{zU_2^n(-z)B_1^{2n+1}(-z)Q(z^2)}{P(z)}. \tag{A.5}$$

We will now show that the decomposition of $g_{(i)}^n$ in (A.1) can be computed from the perfect reconstruction filter bank in Fig. 2 with analysis filters $\mathring{v}$ and $\mathring{w}$.

For this purpose, we need to ensure that the output of the system in Fig. 2 is identical to its input. By using the rules in Table 1, it is not diffcult to show that the z-transform of the output can be written as

$$\tfrac{1}{2}\big(\mathring{V}(z)V(z)+\mathring{W}(z)W(z)\big)C(z) + \tfrac{1}{2}\big(\mathring{V}(z)V(-z)+\mathring{W}(z)W(-z)\big)C(-z), \tag{A.6}$$

where $C(z)\overset{z}{\longleftrightarrow}c_{(i)}(k)$. Hence, we obtain the well known conditions for a perfect reconstruction

$$\begin{aligned}&\mathring{V}(z)V(z)+\mathring{W}(z)W(z)=2,\\ &\mathring{V}(z)V(-z)+\mathring{W}(z)W(-z)=0.\end{aligned} \tag{A.7}$$

Note that the first equation guarantees a distortion free transmission, while the second suppresses aliasing.

We can now attempt to solve this linear system of equations in terms of the unknowns $\mathring{V}(z)$ and $\mathring{W}(z)$. A unique solution for these filters exists if the determinant of the system does not vanish on the unit circle. By replacing $V(z)$ and $W(z)$ by their specific form given by (A.4) and (A.5), we find that the determinant is

$$\Delta(z)=-z\frac{P(z^2)Q(z^2)}{P(z)^2}\big(U_2^n(z)U_2^n(z)B_1^{2n+1}(z) + U_2^n(-z)U_2^n(-z)B_1^{2n+1}(-z)\big),$$

where the right-hand side factor is precisely the z-transform of $2[u_2^n * u_2^n * b_1^{2n+1}]_{\downarrow 2\uparrow 2}(k)$. Next, we use the discrete convolution property of discrete B-splines [43] to show that

$$2[u_2^n * u_2^n * b_1^{2n+1}]_{\downarrow 2\uparrow 2}(k)=4[b_2^{2n+1}]_{\downarrow 2\uparrow 2}(k) \overset{z}{\longleftrightarrow} 4B_1^{2n+1}(z^2),$$

where $b_2^{2n+1}(k)=\beta^{2n+1}(x/2)$. Hence, $\Delta(z)$ simplifies to

$$\Delta(z)=-4z\frac{P(z^2)Q(z^2)B_1^{2n+1}(z^2)}{P(z)^2}. \tag{A.8}$$

We have previously shown that the polynomial $B_1^{2n+1}(z)$ has no zero on the unit circle for all values of n (cf. [2], Proposition 1). The same is obviously true for $P(z)$ and $Q(z)$, which, by definition, represent the z-transforms of invertible convolution operators. Thus, we conclude that $\Delta(z)$ is non-zero for $z=e^{j2\pi f}$. We can then solve the system, which yields

$$\mathring{V}(z)=\frac{2W(-z)}{\Delta(z)}=\frac{1}{2}\frac{U_2^n(z)B_1^{2n+1}(z)P(z)}{P(z^2)B_1^{2n+1}(z^2)}, \tag{A.9}$$

$$\mathring{W}(z)=\frac{-2V(-z)}{\Delta(z)}=\frac{1}{2}\frac{z^{-1}U_2^n(-z)P(z)}{Q(z^2)B_1^{2n+1}(z^2)}. \tag{A.10}$$

It follows that any function $g_{(i)}^n$ can be decomposed as in (A.1) without any loss, which is also equivalent to saying that $W_{(i+1)}^n \oplus V_{(i+1)}^n = V_{(i)}^n$. □

Appendix B. Discrete biorthogonality conditions

Rioul derived the set of conditions (3.33) for the special case of a FIR/FIR perfect reconstruction filter bank [32]. We will extend his results for arbitrary filters. We start by expressing (3.33) in the z-transform domain using the rules in Table 1,

$$\begin{aligned} &\mathring{V}(z)V(z)+\mathring{V}(-z)V(-z)=2,\\ &\mathring{W}(z)W(z)+\mathring{W}(-z)W(-z)=2,\\ &\mathring{V}(z)W(z)+\mathring{V}(-z)W(-z)=0,\\ &\mathring{W}(z)V(z)+\mathring{W}(-z)V(-z)=0. \end{aligned} \tag{B.1}$$

By substituting the general solution given by the central terms in (A.9) and (A.10) in the left-hand side of (B.1) and using the fact that $\Delta(-z)=-\Delta(z)$, we find that the conditions (B.1) are satisfied. Hence (A.7) implies (B.1).

We will now show that (B.1) also implies (A.7) by solving the former set of equations in terms of the unknowns $\mathring{V}(z)$ and $\mathring{W}(z)$. From (B.1), we obtain the two decoupled systems of equations,

$$\begin{bmatrix} V(z) & V(-z)\\ W(z) & W(-z)\end{bmatrix}\begin{bmatrix}\mathring{V}(z)\\ \mathring{V}(-z)\end{bmatrix}=\begin{bmatrix}2\\0\end{bmatrix}, \tag{B.2}$$

$$\begin{bmatrix} W(z) & W(-z)\\ V(z) & V(-z)\end{bmatrix}\begin{bmatrix}\mathring{W}(z)\\ \mathring{W}(-z)\end{bmatrix}=\begin{bmatrix}2\\0\end{bmatrix}. \tag{B.3}$$

The determinant of (B.2) is the same as the determinant of (A.7), i.e.,

$$\Delta(z)=V(z)W(-z)-W(z)V(-z).$$

Assuming that $\Delta(z)$ is non-zero on the unit circle, we find that

$$\begin{bmatrix}\mathring{V}(z)\\ \mathring{V}(-z)\end{bmatrix}=\begin{bmatrix}2W(-z)/\Delta(z)\\ 2W(z)/\Delta(-z)\end{bmatrix}, \tag{B.5}$$

where we once again use the fact that $\Delta(z)=\Delta(-z)$. Similarly, we can solve (B.3) to get

$$\begin{bmatrix}\mathring{W}(z)\\ \mathring{W}(-z)\end{bmatrix}=\begin{bmatrix}-2V(-z)/\Delta(z)\\ -2V(z)/\Delta(-z)\end{bmatrix}. \tag{B.6}$$

In each case, the solutions are mutually compatible and are the same as those given by the central terms in (A.9) and (A.10), respectively. Thus we conclude that conditions (A.7) and (B.1) are equivalent.

References

[1] E.H. Adelson, E. Simoncelli and R. Hingorani, "Orthogonal pyramid transforms for image coding", *Proc. SPIE Conf. Visual Communication and Image Processing*, Cambridge, MA, October, 1987, pp. 50–58.

[2] A. Aldroubi, M. Unser and M. Eden, "Cardinal spline filters: Stability and convergence to the ideal sinc interpolator", *Signal Processing*, Vol. 28, No. 2, August 1992, pp. 127–138.

[3] G. Battle, "A block spin construction of ondelettes. Part I: Lemarié functions", *Commun. Math. Phys.*, Vol. 110, 1987, pp. 601–615.

[4] P. Brodatz, *Textures - A Photographic Album for Artists and Designers*, Dover, New York, 1966.

[5] P.J. Burt, "Fast algorithms for estimating local image properties", *Comput. Graph. Image Process.*, Vol. 21, 1983, pp. 368–382.

[6] P.J. Burt and E.H. Adelson, "The Laplacian pyramid as a compact code", *IEEE Trans. Comm.*, Vol. COM-31, No. 4, April 1983, pp. 337–345.

[7] C.K. Chui and J.Z. Wang, "On compactly supported spline wavelets and a duality principle", *Trans. Amer. Math. Soc.*, Vol. 330, No. 2, 1992, pp. 903–915.

[8] A. Cohen, I. Daubechies and J.C. Feauveau, Biorthogonal bases of compactly supported wavelets, T.M. AT&T Bell Labs, I. Daubechies, 2C371, AT&T Bell Laboratories, 600 Mountain Ave., NJ 07974, 1990.

[9] A. Croisier, D. Esteban and C. Galand, "Perfect channel splitting by use of interpolation, decimation, tree decomposition techniques", *Proc. Internat. Conf. Information Sciences/Systems*, Patras, August 1976, pp. 443–446.

[10] I. Daubechies, "Orthogonal bases of compactly supported wavelets", *Commun. Pure Appl. Math.*, Vol. 41, 1988, pp. 909–996.

[11] J.G. Daugman, "Complete discrete 2-D Gabor transforms by neural networks for image analysis and compression", *IEEE Trans. Acoust. Speech Signal Process.*, Vol. ASSP-36, No. 7, July 1988, pp. 1169–1179.

[12] C. De Boor, *A Practical Guide to Splines*, Springer, New York, 1978.

[13] R. De Valois and K. De Valois, *Spatial Vision*, Oxford Univ. Press, New York, NY, 1988.

[14] P. Flandrin, "Some aspects of non-stationary signal processing with emphasis on time–frequency and time–scale methods", in: J.M. Combes, A. Grossmann and P. Tchamitchian, eds., *Wavelets: Time-Frequency Methods and Phase Space*, Springer, New York, 1989, pp. 68–98.

[15] D. Gabor, "Theory of communication", *J. Inst. Electrical Engrg.*, Vol. 93, No. III, 1946, pp. 429–457.

[16] A. Gersho, 'On the structure of vector quantizers", *IEEE Trans. Inform. Theory*, Vol. IT-28, March 1982, pp. 157–166.

[17] R. M. Gray, "Vector quantization", *IEEE ASSP Mag.*, Vol. 1, April 1984, pp. 4–29.
[18] A. Haar, "Zur Theorie der orthogonalen Funktionensystem", *Math. Ann.*, Vol. 69, 1910, pp. 331–371.
[19] C. Herley and M. Vetterli, "Linear phase wavelets: Theory and design", *Proc. Internat. Conf. Acoust. Speech Signal Processing*, Toronto, Canada, 1991.
[20] E. Kreyszig, *Introduction to Functional Analysis with Applications*, Wiley, New York, 1978.
[21] P.-G. Lemarié, "Ondelettes à localisation exponentielles", *J. Math. Pures Appl.*, Vol. 67, No. 3, 1988, pp. 227–236.
[22] Y.L. Linde, A. Buzo and R.M. Gray, "An algorithm for vector quantizer design", *IEEE Trans. Comm.*, Vol. COM-28, January 1980, pp. 84–95.
[23] T. Lindeberg, "Scale-space for discrete signals", *IEEE Trans. Pattern Anal. Machine Intell.*, Vol. 12, No. 3, March 1990, pp. 234–254.
[24] S.G. Mallat, "Multiresolution approximations and wavelet orthogonal bases of $L^2(R)$", *Trans. Amer. Math. Soc.*, Vol. 315, No. 1, 1989, pp. 69–87.
[25] S.G. Mallat, "A theory of multiresolution signal decomposition: The wavelet representation", *IEEE Trans. Pattern Anal. Machine Intell.*, Vol. PAMI-11, No. 7, 1989, pp, 674–693.
[26] S. Marcelja, "Mathematical description of the responses of simple cortical cells", *J. Opt. Soc. Amer.*, Vol. 70, No. 11, November 1980, pp. 1297–1300.
[27] M.J. Marsden, F.B. Richards and S.D. Riemenschneider, "Cardinal spline interpolation operators on l^p data", *Indiana Univ. Math. J.*, Vol. 24, No. 7, 1975, pp. 677–689.
[28] J. Max, "Quantizing for minimum distortion", *IRE Trans. Inform. Theory*, Vol. IT-6, 1960, pp. 7–12.
[29] Y. Meyer, *Ondelettes et Opérateurs I: Ondelettes*, Hermann, Paris, 1990.
[30] M. Porat and Y.Y. Zeevi, "Localized texture processing in vision: Analysis and synthesis in Gaborian space", *IEEE Trans. Biomed. Engrg.*, Vol. BME-36, No. 1, 1989, pp. 115–129.
[31] P.M. Prenter, *Splines and Variational Methods*, Wiley, New York, 1975.
[32] O. Rioul, "A discrete-time multiresolution theory unifying octave band filter banks, pyramid and wavelet transforms", *IEEE Trans. Signal Process.* to appear.
[33] O. Rioul and M. Vetterli, "Wavelets and signal processing", *IEEE Signal Process. Mag.*, Vol. 8, No. 4, October 1991, pp. 11–38.
[34] I.J. Schoenberg, "Contribution to the problem of approximation of equidistant data by analytic functions", *Quart. Appl. Math.*, Vol. 4, 1946, pp. 45–99, 112–141.
[35] I.J. Schoenberg, "Cardinal interpolation and spline functions", *J. Approximaton Theory*, Vol. 2, 1969, pp. 167–206.
[36] I.J. Schoenberg, "Notes on spline functions III: On the convergence of the interpolating cardinal splines as their degree tends to infinity", *Israel J. Math.*, Vol. 16, 1973, pp. 87–92.
[37] L.L. Schumaker, *Spline Functions: Basic Theory*, Wiley, New York, 1981.
[38] E.P. Simoncelli and E.H. Adelson, "Non-separable extensions of quadrature mirror filters to multiple dimensions", *Proc. IEEE*, Vol. 78, No. 4, 1990, pp. 652–664.
[39] M.J.T. Smith and T.P. Barnwell, "Exact reconstruction for tree-structured subband coders", *IEEE Trans. Acoust. Speech Signal Process.*, Vol. ASSP-34, June 1986, pp. 423–441.
[40] G. Strang, "Wavelets and dilation equations: A brief introduction", *SIAM Rev.*, Vol. 31, 1989, pp. 614–627.
[41] J.O. Strömberg, "A modified Franklin system and higher-order spline system of R^n as unconditional bases for Hardy spaces", *Proc. Conf. Harmonic Analysis in Honor of Antoni Zygmund*, 1983, pp. 475–493.
[42] M.R. Turner, "Texture discrimination by Gabor functions", *Biol, Cybernet.*, Vol. 55, 1986, pp. 71–82.
[43] M. Unser, A. Aldroubi and M. Eden, "Fast *B*-spline transforms for continuous image representation and interpolation", *IEEE Trans. Pattern Anal. Machine Intell.*, Vol. 13, No. 3, March 1991, pp. 277–285.
[44] M. Unser and M. Eden, "Non-linear operators for improving texture segmentation based on features extracted by spatial filtering", *IEEE Trans. Systems Man Cybernet.*, Vol. SMC-20, No. 4, July/August 1990, pp. 804-815.
[45] M. Unser, A. Aldroubi and M. Eden, "Polynomial spline signal approximations: Filter design and asymptotic equivalence with Shannon's sampling theorem", *IEEE Trans. Inform. Theory*, Vol. 38, No. 1, January 1992, pp. 95–103.
[46] M. Unser, A. Aldroubi and M. Eden, "On the asymptotic convergence of *B*-spline wavelets to Gabor functions", *IEEE Trans. Inform Theory*, Vol. 38, No. 2, 1992, pp. 864 872.
[47] M. Unser, A. Aldroubi and M. Eden, "The L_2 polynomial spline pyramic: A discrete multiresolution representation of continuous signals", *IEEE Trans. Pattern Anal. Mach. Intell.*, in press.
[48] M. Vetterli, "Multi-dimensional sub-band coding: Some theory and algorithms", *Signal Processing*, Vol. 6, No. 2, April 1984, pp. 97–112.
[49] M. Vetterli, "A theory of multirate filter banks", *IEEE Trans. Acoust. Speech Signal Process.*, Vol. ASSP-35, No. 3, March 1987, pp. 356–372.
[50] M. Vetterli and C. Herley, "Wavelets and filter banks: Theory and design", *IEEE Trans. Signal Process.*, Vol. 40, No. 9, September 1992, pp. 2207–2232.
[51] P. Witkin, "Scale-space filtering", *Proc. 4th Internat. Joint Conf. Artificial Intelligence*, 1983, pp. 1019–1022.
[52] J.W. Woods and S.D. O'Neil, "Subband coding of images", *IEEE Trans. Acoust. Speech Signal Process.*, Vol. ASSP-34, October 1986, pp. 1278–1288.